RSC Advances

PAPER

View Article Online
View Journal | View Issue

Cite this: *RSC Adv.*, 2019, **9**, 7737

Facile synthesis of g-C_3N_4 with various morphologies for application in electrochemical detection

Wenlian Wang,*[ab] Junming Zhao,[ab] Youyi Sun[c] and Hui Zhang[c]

In the present study, g-C_3N_4 with various morphologies was successfully synthesized *via* a variety of facile *in situ* methods. The as-prepared products were characterized by scanning electron microscopy (SEM), transmission electron microscopy (TEM), Raman spectroscopy and X-ray diffraction (XRD). The results obtained using square wave anodic stripping voltammetry (SWASV) showed that when g-C_3N_4 was applied as an electrochemical sensor, it exhibited excellent sensitivity and selectivity for the detection of heavy metal ions including Pb(II), Cu(II) and Hg(II). Compared to nanoporous graphitic carbon nitride (npg-C_3N_4) and g-C_3N_4 nanosheet-modified glass carbon electrode (GCE), g-C_3N_4 successfully realized the individual and simultaneous detection of four target heavy ions for the first time. In particular, g-C_3N_4 displayed significant electrocatalytic activity towards Hg(II) with a good sensitivity of 18.180 μA μM^{-1} and 35.923 μA μM^{-1} under the individual and simultaneous determination conditions, respectively. The sensitivity for simultaneous determination was almost 2 times that of the individual determination. Moreover, the fabricated electrochemical sensor showed good anti-interference, stability and repeatability; this indicated significant potential of the proposed materials for application in high-performance electrochemical sensors for the individual and simultaneous detection of heavy metal ions.

Received 11th December 2018
Accepted 13th February 2019

DOI: 10.1039/c8ra10166c

rsc.li/rsc-advances

1. Introduction

Heavy metals generally refer to a class of metal elements with atomic density greater than 5 g cm^{-3}. The heavy metals present in aqueous environments usually include lead (Pb), cadmium (Cd), mercury (Hg), copper (Cu), chromium (Cr) and arsenic (As); due to their high toxicity, persistence and non-degradability, heavy metals can easily cause serious effects through their bio-accumulation in the food chain, causing serious harm to human bodies, which in turn results in various diseases of the human body, and environmental pollution.[1–3] Therefore, it is important to develop direct and highly sensitive tools to determine the concentrations of heavy metals in the environment. At present, various methods, such as atomic absorption spectroscopy (AAS), ultraviolet-visible spectrophotometry (UV), X-ray fluorescence spectroscopy (XRF) and inductively coupled plasma mass spectrometry (ICP-MS), have been used for the determination of heavy metal ions. These methods have high sensitivity and selectivity; however, they require expensive instrumentation, complex operational procedures, and long detection time. Moreover, they are neither cost-effective nor user-friendly for routine heavy metal analysis. However, compared with other methods, electrochemical analysis, especially square wave anodic stripping voltammetry (SWASV), has been recognized as a very promising approach for the trace and on-site analysis of heavy metal ions due to its characteristics of simple operation, low detection limit, high sensitivity and good selectivity.[4–7] It can simultaneously detect a variety of heavy metal ions and is generally considered to be an efficient and accurate method for heavy metal analysis. As is known, a key step in electrochemical analysis methods for the detection of heavy metal ions is the design and synthesis of the working electrode materials. Nanomaterials, with a large surface area and plenty of active sites, can improve the analysis efficiency and have been widely utilized to improve the sensing performance of electrochemical detection. Recently, various nanomaterials have been successfully applied for electrochemical determination due to their high adsorption capacity towards heavy metal ions. *Via* functional groups and self-assembly, these materials can be easily assembled on the electrode surface for electrode sensor preparation and have excellent selectivity and sensitivity for the detection for heavy metal ions.[8–11]

In recent years, carbon-based nanomaterials, such as carbon nanomaterials, carbon nanotubes (CNTs), soccer olefins (C_{60}) and graphene, have exhibited excellent electronic properties and are ideal electrode modification materials for heavy metal ion

[a]*Key Laboratory of Instrumentation Science & Dynamic Measurement, Ministry of Education, North University of China, Taiyuan 030051, PR China. E-mail: wangwenlian@nuc.edu.cn*

[b]*National Key Laboratory for Electronic Measurement Technology, North University of China, Taiyuan 030051, PR China*

[c]*Research Center for Engineering Technology of Polymeric Composites of Shanxi Province, North University of China, Taiyuan 030051, PR China*

detection. However, these carbon-based nanomaterials have high cost, restricting their real applications. Similar to graphite, g-C_3N_4 has a layered structure involving weak van der Waals interactions between adjacent C–N layers. g-C_3N_4 has attracted significant attention as a new type of nitrogen-containing carbon material due to its excellent features including good conductivity, large specific surface area, good electrochemical properties and low cost. Thus, it was expected that g-C_3N_4 could be applied in electrochemical detection due to these characteristics.[12–16] Although there are lots of studies on the synthesis and photocatalytic activities of g-C_3N_4 as a photocatalyst, there are only few studies on the synthesis of g-C_3N_4 for successive application in electrochemical detection;[17–24] in addition, g-C_3N_4 with various morphologies, for example, nanoporous graphitic carbon nitride (npg-C_3N_4), g-C_3N_4 bulk and g-C_3N_4 nanosheets, has been synthesized, and it has been reported that it is possible to tune its properties. To date, the effect of morphology on the electrochemical properties of g-C_3N_4 has not been investigated.[25–36]

Based on the abovementioned considerations, g-C_3N_4 with various morphologies, for example bulk, nanoporous and nanosheets, was synthesized for application in the electrochemical detection of heavy metal ions. In addition to this, the remarkable surface area, excellent conductivity and wide electrochemical window have made g-C_3N_4, npg-C_3N_4 and nanosheets of g-C_3N_4 novel materials in the field of electrochemical sensors. Furthermore, the use of square wave anodic stripping voltammetry (SWASV) ensured a fast and high sensitivity current response due to the high electron-transfer speed between the electrode and the solution.

2. Experimental

2.1 Materials

All the reagents were purchased from Sinopharm Chemical Reagent Co., Ltd. (Shanghai, China). Melamine, Triton X-100, H_2SO_4, HNO_3, KCl, $K_3[Fe(CN)_6]$, Nafion (0.25 wt%) and absolute ethanol were of analytical grade and used without further purification. Stock solutions of heavy metal ions, including Pb(II), Hg(II), Cd(II) and Cu(II), used in the experiments for the detection tests were prepared with $Pb(NO_3)_2$, $Hg(NO_3)_2$, $Cd(NO_3)_2$, $Cu(NO_3)_2$, respectively. HAc and NaAc were bought from Tianjin Kemiou Chemical Reagent Co., Ltd. Acetate buffer (0.1 M HAc–NaAc) solutions were prepared by mixing stock solutions of 0.1 M HAc and NaAc·$3H_2O$. They were used as a supporting electrolyte and allowed the circuit to be completed. Deionized water (18.25 MΩ cm) used in the experiments was obtained using an ultra-pure water manufacturing system.

2.2 Preparations of g-C_3N_4

All the chemicals were of analytical grade and used without further treatment. The g-C_3N_4 nanocomposites were prepared following a thermal polycondensation method. At first, 5.0 g melamine was heated to 600 °C under a nitrogen atmosphere. Then, it was allowed to stand for 6 hours to achieve normal temperature, and a light yellow solid was obtained, which was ground to a powder. Finally, an appropriate amount of the powder was taken, and an appropriate amount of secondary deionized water was added to it for sonication for 16 hours; after this, the suspension was allowed to stand for a period of time and then centrifuged in a 5000 rpm centrifuge to obtain larger particles and g-C_3N_4 bulk. The sample was usually labeled as g-C_3N_4.

Npg-C_3N_4 was synthesized by a template-induced method according to a previous study.[37] In a typical synthetic procedure, first, 5.0 g melamine and 2.5 g Triton X-100 were heated in an oil bath at 100 °C under stirring for 1 h. Then, the right amount of concentrated sulfuric acid (98 wt%) was added, a white precipitate gradually formed, and the mixture was then stirred at 100 °C for another hour. After being naturally cooled down to room temperature, the precipitate was filtered, washed several times to remove Triton X-100 and then dried at 80 °C. The obtained sample was heated to 500 °C in a muffle furnace for 2 h at the heating rate of 2 °C min^{-1}, and further heat treatment was then performed at 580 °C for another 2 h.

We have adopted an aqueous phase exfoliation method for the preparation of g-C_3N_4 nanosheets.[38] Herein, 0.5 g bulk g-C_3N_4 was stirred for 1 h and then ultrasonicated for 10 h in a hot water bath. To maintain the temperature near room temperature, ice cubes were added to the water at regular intervals of time. The aqueous dispersed carbon nitride nanosheets formed were centrifuged at 5000 rpm. The supernatant was again centrifuged at 18 000 rpm to obtain g-C_3N_4 nanosheets.

2.3 Apparatus and characterization

All the electrochemical measurements were performed using the CHI660E computer-controlled potentiostat (ChenHua Instrument Co., Shanghai, China). Experiments were conducted in a conventional three-electrode system using a modified bare glass carbon electrode (GCE) as the working electrode, Ag/AgCl/saturated KCl as the reference electrode and platinum wire as the counter electrode. The morphology and phase structure of the samples were investigated by a field emission scanning electron microscope (FESEM, Hitachi S-4800). High-resolution transmission electron microscopy (HRTEM) observation was carried out using the JEM-2010 microscope (JEOL, Japan). X-ray diffraction (XRD) patterns of the g-C_3N_4 nanocomposites with various morphologies were acquired using the Horiba EX-250 X-ray energy-dispersive spectrometer (EDS). Raman spectra were obtained using the Jobin-Yvon LabRam HR800 Raman spectroscope equipped with a 514.5 nm laser source.

2.4 Electrochemical characterization

2.4.1 Working electrode pretreatment process. Pretreatment of the working electrode was a more critical step in this experiment. To form a mirror-shiny surface, the bare GCE was carefully polished on felt pads with 1.0 μm, 0.3 μm and 0.05 μm alumina slurry in sequence and cleaned by deionized water afterwards. Then, the GCE was sonicated with HNO_3 (1 : 1, v/v), absolute ethanol and deionized water in sequence for certain time to reduce the amount of the adsorbed substances on the surface of the electrode. After this, the treated electrode was dried with a stream of nitrogen gas. Then, 5 mg of g-C_3N_4 was dispersed in 2 mL of Nafion (0.25 wt%) and absolute ethanol

mixed solutions. The solution was ultrasonically dispersed in a weighing bottle for 30 minutes. The next most important step was to add the material to the working electrode. A certain amount of g-C_3N_4 mixture was added to the surface of the working electrode with a pipette of corresponding specifications (0.5–50 μL, sampling 2 μL each time), and the working electrode was placed in a blast drying oven for drying. To facilitate comparison, npg-C_3N_4 and nanosheets of g-C_3N_4-modified GCE were also prepared following the same procedure.

2.4.2 Electrochemical measurements. All the experiments were conducted by the cyclic voltammetry method: the scanning was from −0.1 to 0.6 V; the amplitude was 20 mV; the step height potential was 5 mV; the time of integration was 2 ms; and the frequency was 25 Hz. To realize individual and simultaneous detections of Pb(II), Hg(II), Cd(II) and Cu(II), square wave anodic stripping voltammetry (SWASV) is the most commonly used electrochemical measurement method; at first, the working electrode has been modified with a modified material by putting it into a mixture solution including 0.1 M HAc–NaAc and heavy metal ions. Then, heavy metal ions have been deposited on the surface of the working electrode at the potential of −1 V *vs.* SCE for 150 s. For the enrichment process, the metal ions have been reduced through a reduction reaction. In the dissolution process, the heavy metal was originally deposited on the electrode in an ionic state and returned to the solution through an oxidation reaction. Since the positions of the dissolution peaks of different heavy metal ions were different, the parameter setting was performed according to the heavy metal ions. Furthermore, a positive potential was applied to the clean working electrode for 300 s to remove the deposited residual heavy metal ions from the surface after each detection experiment.

3. Results and discussion

The formation of g-C_3N_4 with various morphologies was confirmed by the XRD pattern and FTIR spectra shown in Fig. 1A and B, respectively. All the samples clearly showed two similar characteristic peaks of 14.8° and 27.5°, as shown in Fig. 1A, which were ascribed to the (100) and (002) planes of g-C_3N_4, respectively. The results indicated the formation of g-C_3N_4. In comparison, compared with those of npg-C_3N_4 and g-C_3N_4 bulk, the peak intensity assigned to the (100) plane of g-C_3N_4 was enhanced. On the contrary, there was a relatively weaker peak at $2\theta = 27.5°$, corresponding to the plane nitrogen hole spacing (d = 0.672 nm) formed by the tri-*s*-triazine structure.[24–35] These results indicated the formation of g-C_3N_4 nanosheets. As shown in Fig. 1B, all the samples showed similar FTIR absorption spectra. The absorption peak was assigned to the stretching vibration of N–H at around 3660.0 cm^{-1}. Moreover, five characteristic peaks at 847.0, 1220.0, 1316.0, 1550.0 and 1660.0 cm^{-1} were attributed to the skeletal vibrations of tris triazine ring units of g-C_3N_4. The signal at 1390.0 cm^{-1} was assigned to the stretching vibrations of the *s*-triazine ring units.[24–28] These results indicated that the *s*-triazine and tris triazine ring units simultaneously existed in the g-C_3N_4 prepared using urea precursors. Note that the FTIR spectra of npg-C_3N_4 and nanosheets of g-C_3N_4 were similar to that of g-C_3N_4; this suggested that they maintained the same chemical structure as their parent counterpart.

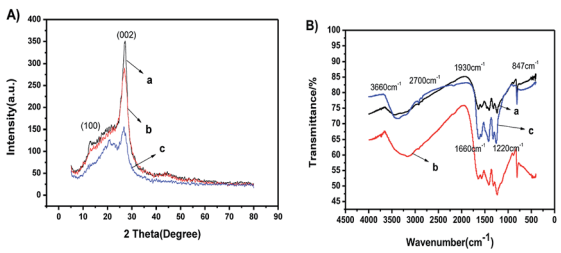

Fig. 1 (A) XRD patterns and (B) FTIR spectra of (a) g-C_3N_4, (b) npg-C_3N_4 and (c) nanosheets of g-C_3N_4.

The micro-structure of g-C_3N_4 with various morphologies was further characterized by SEM and TEM images, as shown in Fig. 2. As shown in Fig. 2a–c, all the samples showed a typical layered platelet-like morphology. In addition, they showed large amounts of aggregation with a layered structure.[24–35] The elemental mapping images and energy-dispersive X-ray spectrometer (EDS) results of g-C_3N_4 are shown in Fig. 2d. The elements C and N were obviously detected and uniformly distributed within the sample. To further prove the molecular composition of g-C_3N_4, EDS spectra of g-C_3N_4 was used to detect the content and mass ratio of C, N, and O elements, as shown in Fig. 3, and the C and N contents of g-C_3N_4 were calculated to be 39.718% and 60.082%, respectively, according to the weight ratio of these elements. These results indicated that the C : N ratio was almost 3 : 4. The formation of g-C_3N_4 nanosheets was further characterized by the TEM images, as shown in Fig. 2e, showing a nanosheet-like morphology. Fig. 4a–c represent the N_2 isothermal adsorption and desorption experimental results for g-C_3N_4, npg-C_3N_4 and nanosheets of g-C_3N_4. According to the IUPAC classification model, the shapes of the nitrogen isothermal adsorption belonged to IV-type cure and H3 hysteresis loop. Moreover, the pore sizes of g-C_3N_4, npg-C_3N_4 and nanosheets of g-C_3N_4 were 1.917, 1.923 and 1.915 nm, and the specific surface areas of g-C_3N_4, npg-C_3N_4 and nanosheets of g-C_3N_4 were 30.393, 26.651 and 37.886 $m^2\ g^{-1}$, respectively. Although the nanosheets of g-C_3N_4 had largest specific surface area, their pore size was smallest. These results further confirmed the findings for g-C_3N_4.

CV and EIS have been widely used for the characterization of modified electrodes, which provide clearer information about the electron-transfer kinetics of redox probes. The electrochemical characterization results of the bare glassy carbon electrode and modified materials are shown in Fig. 5a. Compared with the case of the bare glassy carbon electrode, it could be indicated that the oxidation peak and the reduction peak current of the modified electrode of g-C_3N_4, npg-C_3N_4 and nanosheets of g-C_3N_4 respectively decreased, whereas the peak-to-peak separations were widened in the cyclic voltammetry (CV) curves; this was because the modified materials on the surface of the electrode hindered the transfer of electrons and had poor electrical conductivity. Fig. 5b shows the corresponding electrochemical impedance spectra (EIS). Typically,

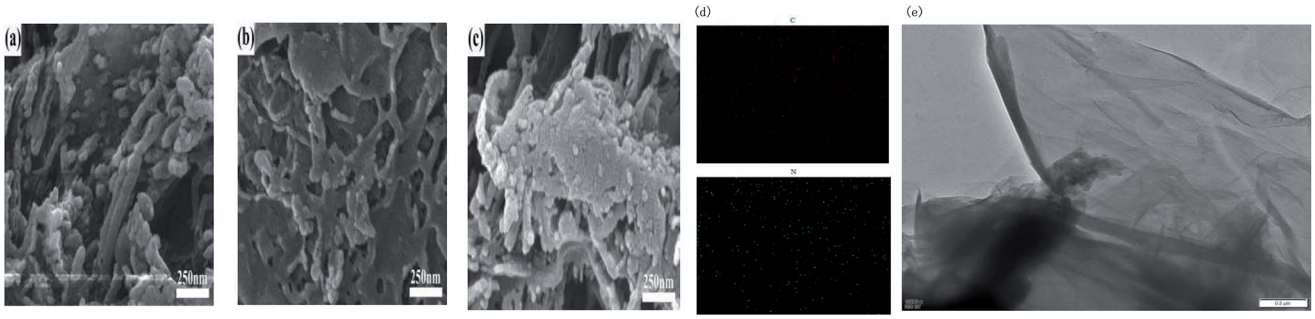

Fig. 2 SEM images of (a) g-C_3N_4, (b) npg-C_3N_4 and (c) nanosheets of g-C_3N_4; (d) elemental mapping images and energy-dispersive X-ray spectrometer (EDS) results of g-C_3N_4; and (e) TEM images of the g-C_3N_4 nanosheets.

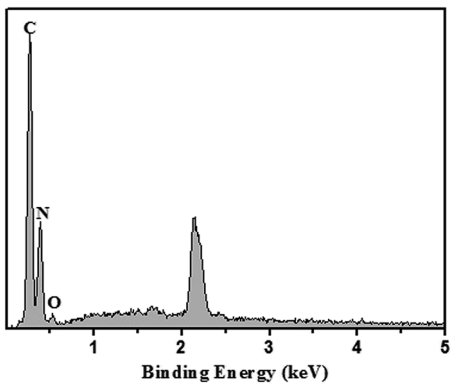

Fig. 3 EDS spectra of g-C_3N_4.

the electrochemical impedance spectra consisted of two parts: a straight line portion and a semicircular portion, which were respectively in the high frequency region and the low frequency region. The values corresponding to the semicircular diameter indicated the corresponding electron-transfer resistance, and the straight line portion represented the electron-diffusion process. The interface properties of the modified electrodes obtained using different materials were further confirmed through EIS. As shown in Fig. 5b, g-C_3N_4, npg-C_3N_4 and the nanosheets of g-C_3N_4 respectively modified the R_{et} of the electrode, and the electrochemical impedance spectra of the bare glassy carbon electrode was almost a straight line. Equivalent circuit plots in the EIS data fitting are shown in the inset of Fig. 5b, where R_s represents the sum of the ohmic resistance, including the ohmic resistance of the electrolyte, the electrode and the interface, of the research system; C_{d1} and C_{d2} represent the double layer capacitance and the capacitance of the SEI film instead of a capacitor to compensate for non-homogeneity in the system; and R_1 and R_2 are charge-transfer resistors. This further indicated that g-C_3N_4, npg-C_3N_4 and nanosheets of g-C_3N_4 hindered the transfer of electrons on the electrode surface, and the electrochemical catalytic behavior was better after modification of the electrode surface. This may be attributed to the high activity of g-C_3N_4, npg-C_3N_4 and nanosheets of g-C_3N_4. Moreover, as can be seen from the EIS data, the nanosheets of g-C_3N_4 had highest equivalent resistance (R_{et} >30 Ω) in the high-frequency region, whereas npg-C_3N_4 had the worst diffusion effect in the low-frequency region. These results showed that the lamellar structure of g-C_3N_4 had the advantage of increasing the specific surface area and accelerating the migration rate of electrons. The result was consistent with the CV data of different electrodes.

To obtain higher detection sensitivity and low detection limit, experiments were performed under optimal conditions, and the modified electrodes were tested under the same conditions. Optimal conditions were obtained by the method of controlling a single variable. The SWASV response towards Pb(II) detection on g-C_3N_4, npg-C_3N_4 and g-C_3N_4 nanosheet-modified GCE was determined in an electrolyte solution of 0.1 M HAc–NaAc (pH = 5) at the deposition potential of −1.0 V for 150 s, and the results are shown in Fig. 6a–c. Corresponding

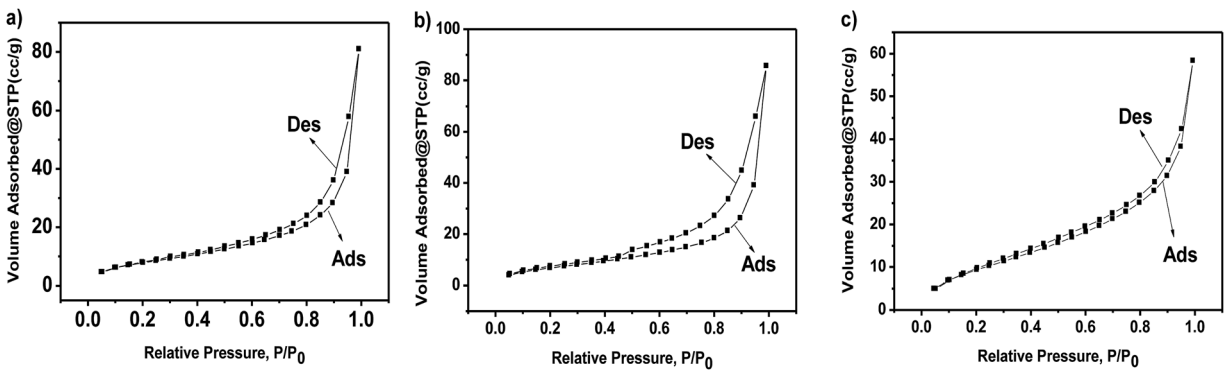

Fig. 4 N_2 isothermal adsorption of (a) g-C_3N_4, (b) npg-C_3N_4 and (c) npg-C_3N_4.

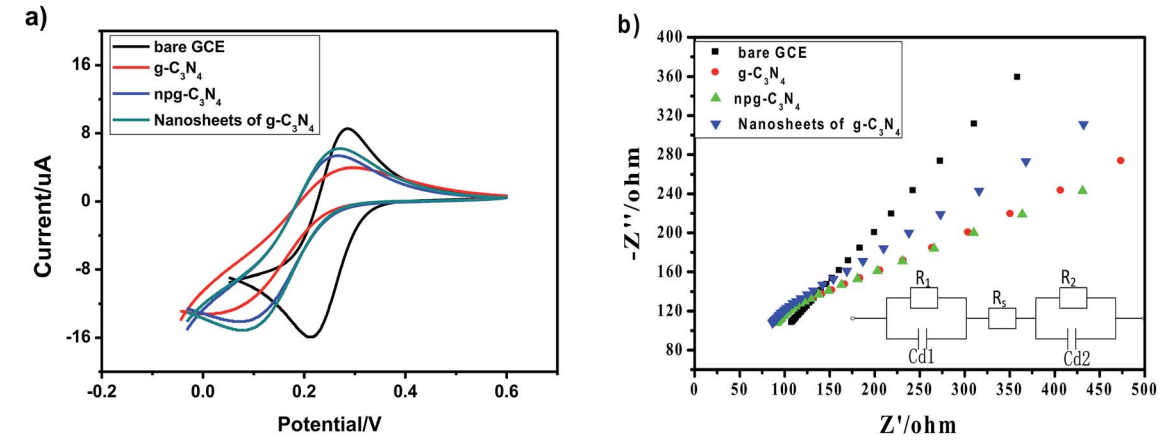

Fig. 5 (a) Cyclic voltammetric responses and (b) electrochemical impedance spectra of bare GCE; g-C_3N_4, npg-C_3N_4 and nanosheets of g-C_3N_4-modified GCE in an electrolyte solution of 0.1 M KCl and 5 mM $K_3[Fe(CN)_6]$ (inset figure shows the equivalent circuit plots in the EIS data fitting). Scan rate: 100 mV s^{-1}, polarization potential: 0.25 V, frequency spectra 1–100 000 Hz.

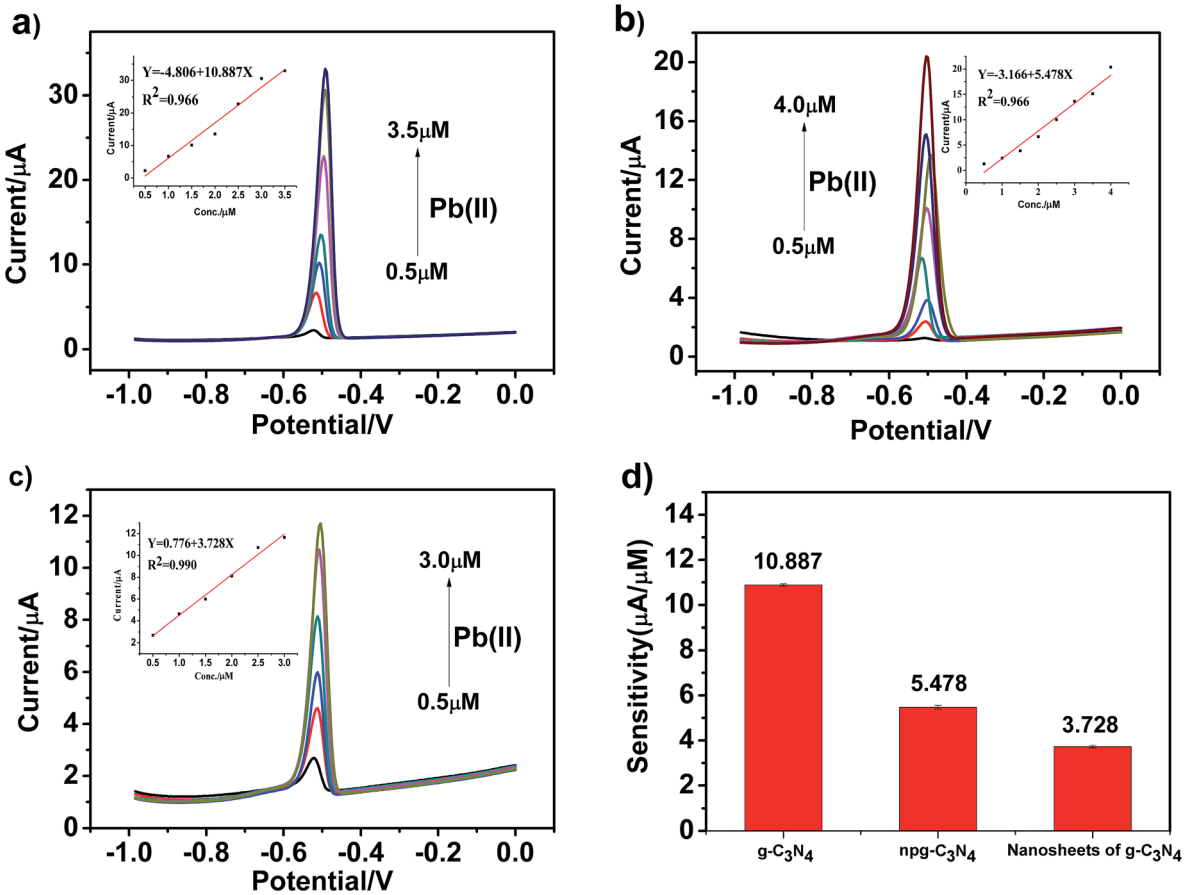

Fig. 6 (a–c) SWASV response towards Pb(II) detection on g-C_3N_4, npg-C_3N_4 and g-C_3N_4 nanosheet-modified GCE in an electrolyte solution of 0.1 M HAc–NaAc (pH = 5) at the deposition potential of −1.0 V for 150 s. The potential step is 5 mV, the amplitude is 20 mV, and the frequency is 25 Hz. (d) Comparison between the sensitivity *versus* Pb(II) for the modified electrodes based on the different materials considered in this study.

to the electrochemical detection of Pb(II), an obvious peak was observed at about −0.5 V. The stripping current increased as the concentration of the metal ions increased. Moreover, significantly different sensitivities towards Pb(II) detection were associated with each modified electrode material. Obviously, the Pb(II) detection sensitivity of g-C_3N_4 was highest. It could be observed that the sensitivity for the analysis of Pb(II) was as follows: g-C_3N_4 > npg-C_3N_4 > nanosheets of g-C_3N_4. The linearization equation was $i/\mu A = -4.806 + 10.887c/\mu M$ with a correlation coefficient of 0.966 over the respective concentration ranges from 0.5 to 3.5 μM (inset of Fig. 6a), and the limit of detection (LOD) was calculated to be 0.228 μM (*via* the 3σ

method), as shown in Fig. 6d. The linearization equation for the npg-C_3N_4-modified GCE was $i/\mu A = -3.166 + 5.478c/\mu M$ with a correlation coefficient of 0.966 over the concentration range from 0.5 to 4.0 μM (inset of Fig. 6b). The linearization equation for the nanosheets of g-C_3N_4 was $i/\mu A = 0.776 + 3.728c/\mu M$ with a correlation coefficient of 0.986 over the concentration range from 0.5 to 3.0 μM (inset of Fig. 6c). Overall, the g-C_3N_4-modified GCE obtained higher detection sensitivity and low detection limit towards Pb(II) detection, which was selected for the subsequent detection of multiple heavy metal ions.

Similarly, we used the same method to separately detect other heavy metal ions and obtained the detection sensitivity and detection limit of different modified materials for other heavy metal ions. Fig. 7a–c present the SWASV response towards Hg(II) detection on g-C_3N_4, npg-C_3N_4 and g-C_3N_4 nanosheet-modified GCE over different concentration ranges of equal concentration gradient in 0.1 M HAc–NaAc (pH = 5). The Hg(II) peak was visible at about +0.35 V. The linearization equations of g-C_3N_4, npg-C_3N_4 and nanosheets of g-C_3N_4 for the detection of Hg(II) were $i/\mu A = -11.781 + 18.180c/\mu M$ ($R^2 = 0.959$) with the limit of detection (LOD) of 0.217 μM (3σ method), $i/\mu A = -3.733 + 6.976c/\mu M$ ($R^2 = 0.957$), and $i/\mu A = -17.131 + 1\,3.485c/\mu M$ ($R^2 = 0.991$), respectively. It could be observed that the sensitivity for analysis of Hg(II) was as follows: g-C_3N_4 > nanosheets of g-C_3N_4 > npg-C_3N_4. On the one hand, g-C_3N_4 may possess more excellent adsorption capacity and exhibit higher catalytic activity towards Hg(II) than the other heavy ions during the oxidation reduction process of SWASV. On the other hand, g-C_3N_4 has a layered structure similar to that of graphene, and a mercury film can be formed on the surface of the electrode, which can increase the deposition amount of Hg(II) on the surface of the electrode and improve the electronic transfer. Therefore, g-C_3N_4 demonstrated very high selectivity towards Hg(II).

Fig. 8a–c present the SWASV response toward Cu(II) detection on g-C_3N_4, npg-C_3N_4 and g-C_3N_4 nanosheet-modified GCE over different concentration ranges of an equal concentration gradient in 0.1 M HAc–NaAc (pH = 5). Well-defined peaks were obvious at about 0 V, and the nanosheets of g-C_3N_4 had better sensitivity to detect Cu(II) than g-C_3N_4 and npg-C_3N_4. The linearization equation for the nanosheets of g-C_3N_4 was $i/\mu A = -3.017 + 5.151c/\mu M$ with a correlation coefficient of 0.959 over the respective concentration ranges from 0.5 to 4.5 μM (inset of Fig. 8c), and the limit of detection (LOD) was calculated to be 0.103 μM (*via* the 3σ method). A comparison between the sensitivities of the modified electrodes based on different materials towards Pb(II), Hg(II) and Cu(II) is shown in Fig. 8d. It could been seen that the g-C_3N_4-modified electrodes used to

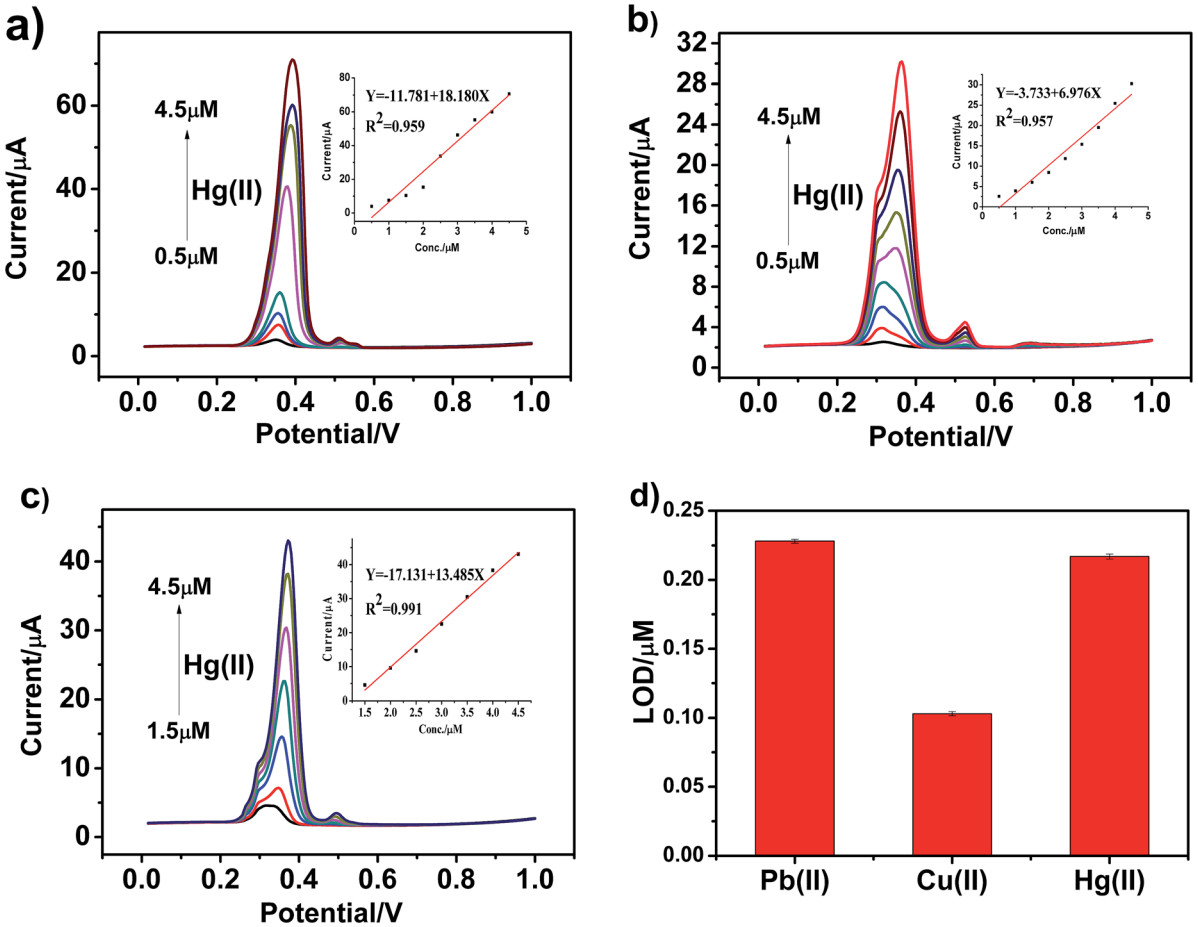

Fig. 7 (a–c) SWASV response towards Hg(II) detection on g-C_3N_4,npg-C_3N_4 and g-C_3N_4 nanosheet-modified GCE in an electrolyte solution of 0.1 M HAc–NaAc (pH = 5) at the deposition potential of −1.0 V for 150 s. The potential step is 5 mV, the amplitude is 20 mV, and the frequency is 25 Hz. (d) Comparison of LODs of Pb(II), Cu(II) and Hg(II) on the g-C_3N_4-modified electrodes.

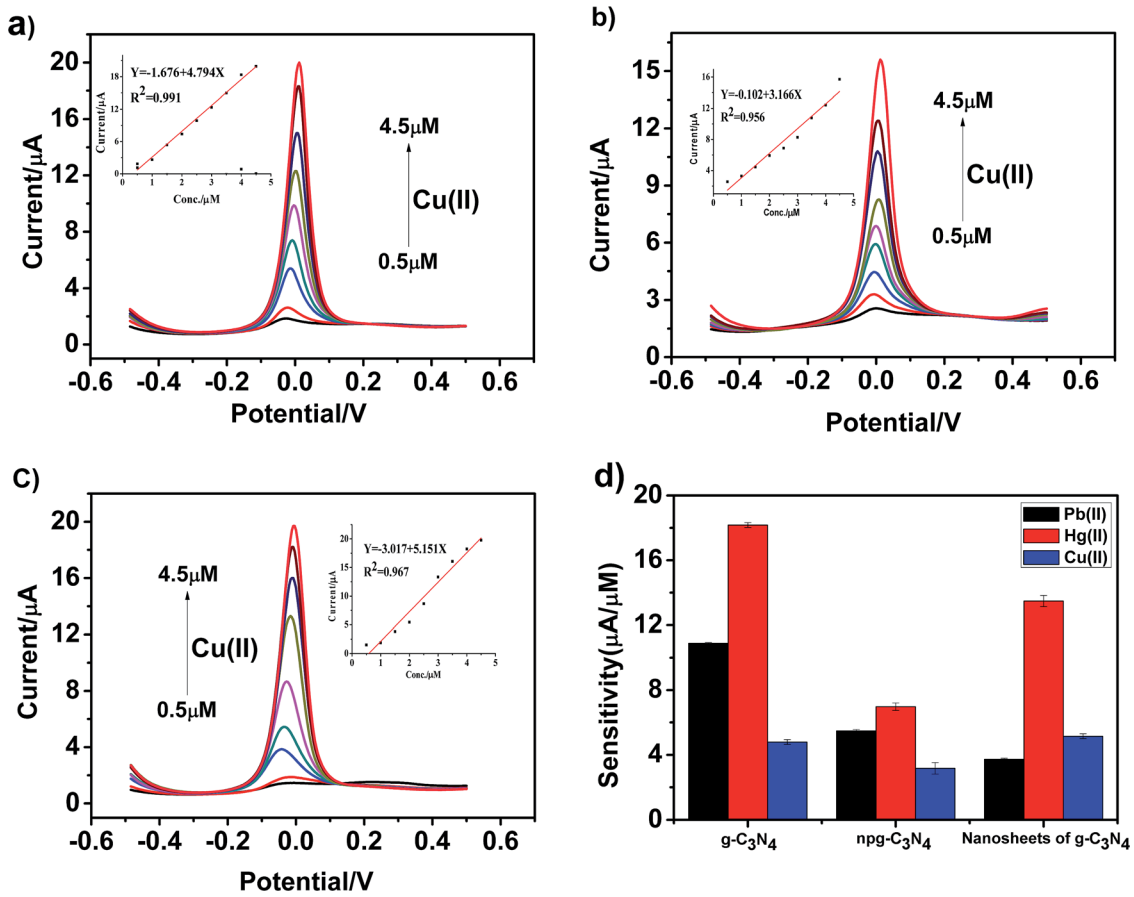

Fig. 8 (a–c) SWASV response toward Cu(II) detection on g-C_3N_4, npg-C_3N_4 and g-C_3N_4 nanosheet-modified GCE in an electrolyte solution of 0.1 M HAc–NaAc (pH = 5) at the deposition potential of −1.0 V for 150 s. The potential step is 5 mV, the amplitude is 20 mV, and the frequency is 25 Hz. (d) Comparison between the sensitivities of the modified electrodes based on the different materials considered in this study towards Pb(II), Hg(II) and Cu(II).

detect three heavy metal ions individually showed good electrochemical performance, especially towards Pb(II) and Hg(II). The results indicated that g-C_3N_4 had large specific surface area and more active sites, which were beneficial for its binding to heavy metal ions and chemical reactions.

The Pb(II) and Hg(II) detection performance of the proposed sensor was compared with those of other previously reported modified electrodes, and the results are summarised in Table 1. It was observed that preferable sensitivity with a low LOD was obtained at the g-C_3N_4-modified electrode. The results demonstrated that high sensitivity towards Pb(II) and Hg(II) could be obtained at the g-C_3N_4-modified electrode. Compared with the other GCE-modified materials reported previously, g-C_3N_4 displayed much higher sensitivity and even achieved the same effect as poly(BPE)/g-C_3N_4; moreover, it was very simple and easy to prepare. Therefore, it may provide useful insights into the design of high-performance electrochemical sensors applied in the individual and simultaneous detection of heavy metal ions.

As shown in Fig. 9a–c, heavy metal ions, including Cd(II), Pb(II), Cu(II) and Hg(II), at different concentrations were simultaneously detected under similar conditions using the g-C_3N_4, npg-C_3N_4 and g-C_3N_4 nanosheet-modified GCE. The individual stripping peaks for Cd(II), Pb(II), Cu(II) and Hg(II) could be clearly observed at −0.70, −0.50, 0 and +0.30 V, respectively. These results showed that the simultaneous and individual detection of the four considered heavy metal ions resulted in well-separated stripping peaks. Moreover, the potential separation between these stripping peaks was clear enough to distinguish the four

Table 1 Comparison of the current sensitivity and LOD with those of the previously reported electrodes for electrochemical determination

Ions	Electrodes	Sensitivity (μA μM^{-1})	LOD (μM)	Ref.
Pb(II)	g-C_3N_4	10.887	0.228	This work
	Npg-C_3N_4	5.478	0.211	This work
	Nanosheets of g-C_3N_4	3.728	0.121	This work
	Poly(BPE)/g-C_3N_4	11.139	—	39
	CN-NS/Nafion/GCE	—	0.230	40
	poMWCNTs	3.55	0.057	41
	NH_2-MIL-88(Fe)-rGO	0.05	0.001	42
	MnO_2 NPs/rGO	4.42	0.075	43
	$MgSiO_3$/Nafion GCE	9.44	—	44
Hg(II)	g-C_3N_4	18.180	0.103	This work
	Npg-C_3N_4	6.976	0.276	This work
	Nanosheets of g-C_3N_4	13.485	0.154	This work
	Fe_3O_4@C nanosphere	0.91	—	45
	$MnFe_2O_4$@Cys	11.7	0.208	8
	AuNPs/rGO	3.28	0.08	46
	Ut g-C_3N_4	6.084	0.023	47

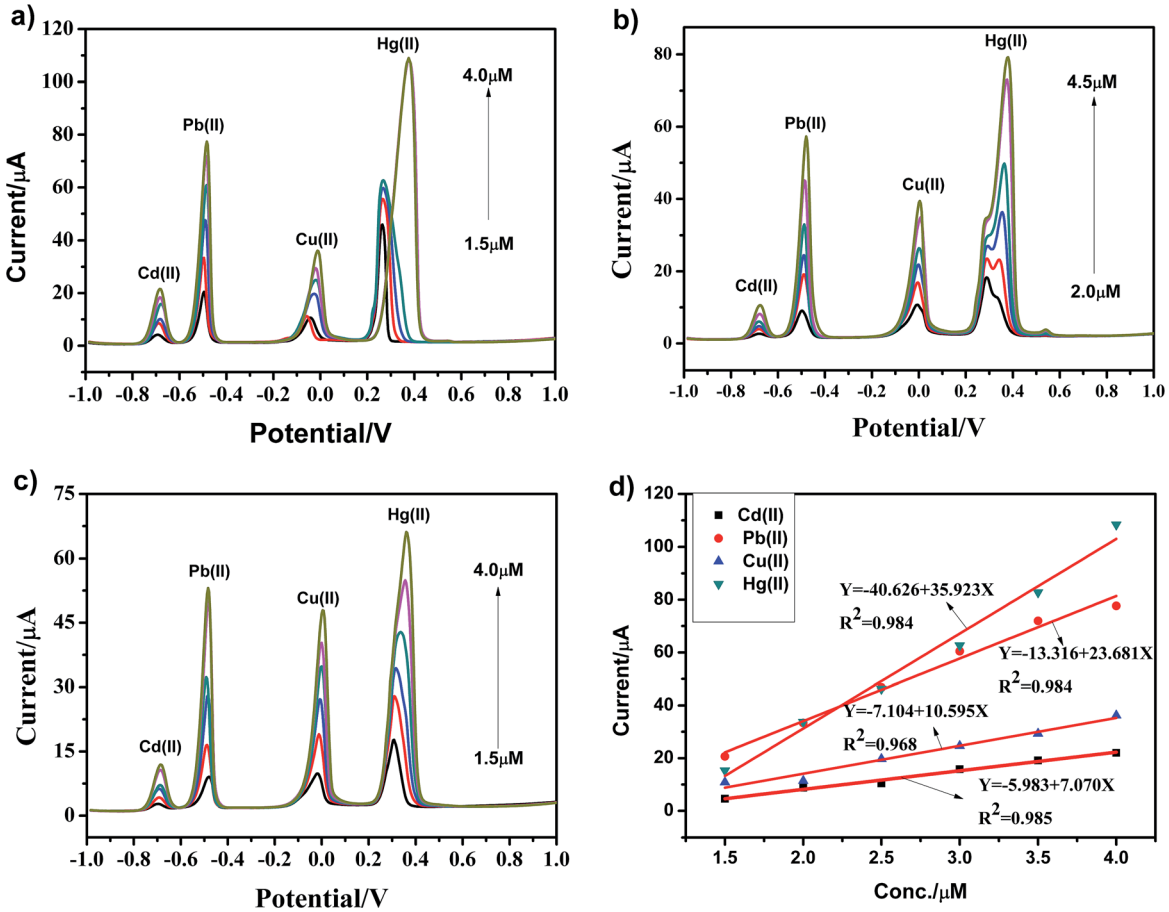

Fig. 9 (a–c) SWASV responses towards the g-C_3N_4, npg-C_3N_4 and g-C_3N_4 nanosheet-modified GCE for the simultaneous detection of Cd(II), Pb(II), Cu(II) and Hg(II) over a certain concentration range. (d) Calibration plots towards Cd(II), Pb(II), Cu(II) and Hg(II) obtained using the g-C_3N_4-modified GCE. Deposition potential: −1 V, amplitude: 20 mV, frequency: 25 Hz and *vs.* Ag/AgCl/KCl (3 M KCl saturated with AgCl).

heavy metal ions. Fig. 9d shows the calibration plots towards Cd(II), Pb(II), Cu(II) and Hg(II) obtained using the g-C_3N_4-modified GCE. Obviously, it could be observed that the sensitivity for analysis was as follows: Hg(II) > Pb(II) >Cu(II) > Cd(II). The linearization equation for Hg(II) over the respective concentration ranges from 1.5 to 4.0 μM was $i/\mu A = -40.626 + 35.923c/\mu M$ with a correlation coefficient of 0.984. In addition, the linearization equations for Pb(II) and Cu(II) were $i/\mu A = -13.316 + 23.681c/\mu M$ ($R^2 = 0.984$) and $i/\mu A = -7.104 + 10.595c/\mu M$ ($R^2 = 0.968$), respectively. With an increase in the concentration of heavy metal ions, the enrichment potential of the oxidation peak gradually shifted to the positive direction, and the peak current also increased positively in a certain interval. To better analyze the interference of these four metal ions, Table 2 displays the sensitivity, correlation coefficient, and calculated LODs for the individual and simultaneous detection of heavy metal ions. As the concentration of heavy metal ions increased, Cd(II), Pb(II), Cu(II) and Hg(II) were significantly enhanced; this could be ascribed to the presence of a Hg film and a mutual promotion between heavy metal ions during the enrichment process. To date, due to the environment-friendliness of the hanging mercury drop electrode (HMDE), it has been widely applied to improve the detection sensitivity. In our experiment, there was no obvious stripping peak for the bare glassy carbon electrode when compared with the stripping peaks of Cd(II), Pb(II), Cu(II) and Hg(II) using the g-C_3N_4-modified GCE.

The stability of electrode and experimental repeatability are also very important for practical application in electrochemical detection. A repeatability study of the g-C_3N_4-modified GCE was thus carried out in a parallel experiment 10 times once a day. We selected Pb(II) as the target heavy metal ion. The SWASV responses towards the g-C_3N_4-modified GCE in 0.1 M HAc–NaAc (pH = 5) containing 4 μM Pb(II) after 10 successive scans are shown in Fig. 10a. The peak values of the oxidation peak were about 39 μA. This clearly showed that the peak current slightly changed as the number of trials increased; this indicated that

Table 2 Comparison of the individual and simultaneous analysis conducted using g-C_3N_4

	Analyte	Sensitivity (μA μM^{-1})	Correlation coefficient	LOD (μM)
Individual analysis	Pb(II)	10.887	0.966	0.228
	Cu(II)	4.794	0.991	0.103
	Hg(II)	18.180	0.959	0.217
Simultaneous analysis	Pb(II)	23.681	0.984	0.168
	Cu(II)	10.595	0.968	0.243
	Hg(II)	35.923	0.984	0.170

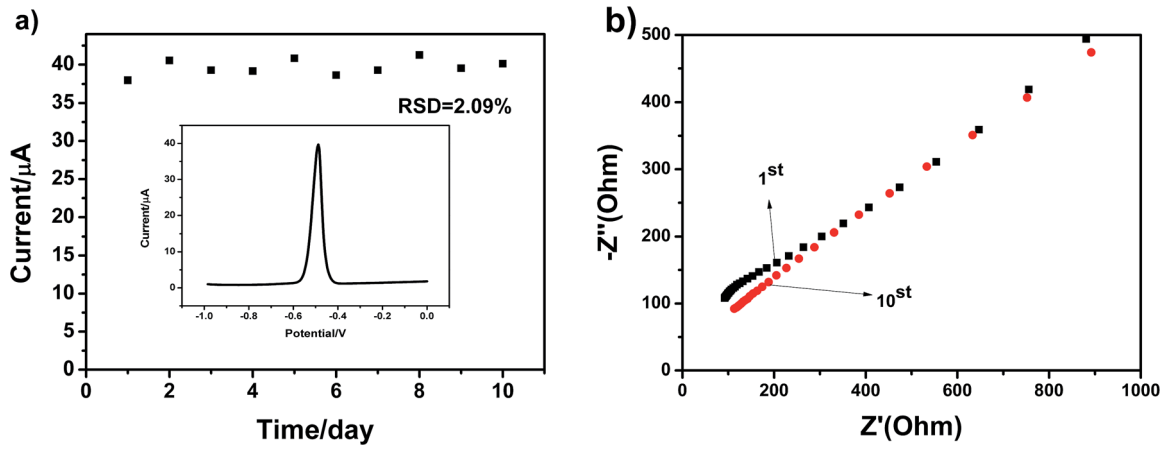

Fig. 10 (a) Repeatability study of g-C_3N_4 in 0.1 M HAc–NaAc (pH = 5) containing 4 μM Pb(II). Deposition potential: 1 V; amplitude: 25 mV; increment potential: 4 mV; frequency: 15 Hz; *vs.* Ag/AgCl, and (b) EIS data of the g-C_3N_4 electrode towards Pb(II) from the 1st cycle to 10th cycle.

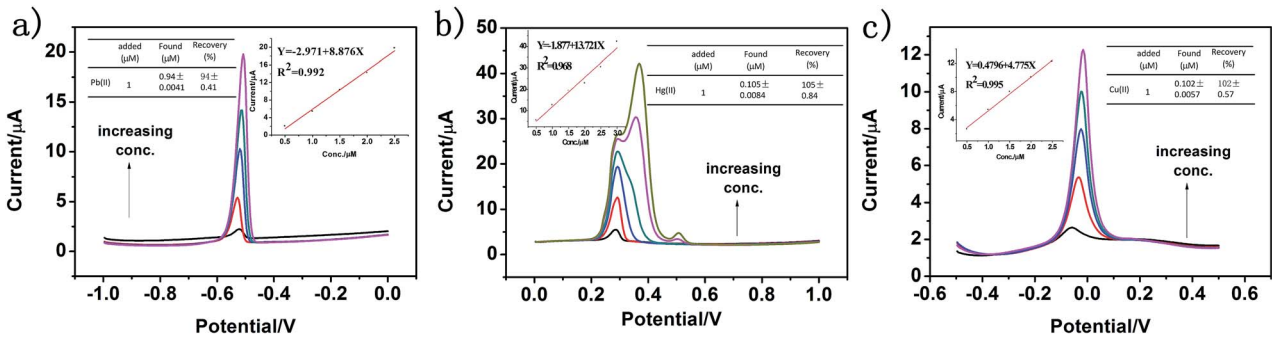

Fig. 11 (a–c) SWASV responses of g-C_3N_4 towards Pb(II), Hg(II) and Cu(II) in real water samples diluted with 0.1 M NaAc-HAc solution (pH 5.0) in a ratio of 1 : 4 obtained by the standard addition method and the corresponding calibration plot of the peak current against the three heavy metal ion concentrations (inset).

the repeatability of the fabricated electrochemical sensor was particularly good. The EIS results for the g-C_3N_4 electrode are shown Fig. 10b towards Pb(II) from the 1st cycle to the 10th cycle. As can be seen, as the number of days increases, the diffusion effect slowly decreases. Overall, it can be seen that the stripping currents on g-C_3N_4-modified GCE are nearly steady, and the relative standard deviation (RSD) has been calculated to be 2.09%. These results indicate that the g-C_3N_4-modified GCE displays excellent cycling stability and long-term durability for repeated electrochemical determination, which offer a very broad application prospect.

To evaluate the accuracy of the proposed sensor in practical application, g-C_3N_4 was applied for monitoring Pb(II), Hg(II) and Cu(II) in real water samples diluted with 0.1 M HAc–NaAc buffer solution (pH 5.0) in a ratio of 1 : 4 by a standard addition method, and the results are shown in Fig. 11a–c. The real water sample was obtained from the Fen River water in Taiyuan City (Shanxi Province, China). It can be seen that there is no obvious current signal when the electrodes modified by g-C_3N_4 are directly used to determine Pb(II), Hg(II) and Cu(II) in the treated real water sample. Then, Pb(II), Hg(II) and Cu(II) at different concentrations were added, and a sharp stripping peak could be observed. As shown in Fig. 11a–c, it was clear that the found concentrations of Pb(II), Hg(II) and Cu(II) were well consistent with the added amount, and the recovery of Pb(II), Hg(II) and Cu(II) was 94%, 105%, and 99% with the RSD of 0.41%, 0.84%, and 0.57%, respectively. This result shows that the proposed electrochemical sensor is applicable for the detection of heavy metal ions in real water samples.

4. Conclusion

In this study, g-C_3N_4, npg-C_3N_4 and nanosheets of g-C_3N_4 were successfully synthesized by a variety of facile methods. Moreover, the effect of the morphology of these different materials on the electrochemical detection of heavy metal ions was investigated in detail. CV and EIS results showed that the modification by g-C_3N_4, npg-C_3N_4 and nanosheets of g-C_3N_4 could enhance the electrochemical activity. The results obtained using square wave anodic stripping voltammetry (SWASV) showed that g-C_3N_4 applied as an electrochemical sensor exhibited excellent sensitivity and selectivity for the detection of heavy metal ions including Pb(II), Cu(II) and Hg(II). The sensitivities were 10.887, 4.794, and 18.180 μA μM^{-1} and the limits of detection (LOD) were 0.228, 0.103, and 0.217 μM, respectively. Compared to npg-C_3N_4 and g-C_3N_4 nanosheet-modified glass carbon electrode (GCE), g-C_3N_4 successfully realized the individual and simultaneous detection towards four target heavy ions for the first time. In particular, g-C_3N_4 displayed significant electrocatalytic activity towards Hg(II)

with a good sensitivity of 18.180 μA μM^{-1} and 35.923 μA μM^{-1} under the individual and simultaneous determination conditions, respectively. The sensitivity for simultaneous determination was almost 2 times that of individual determination. Moreover, the fabricated electrochemical sensor showed good anti-interference, stability and repeatability, which greatly promoted its potential usage in high-performance electrochemical sensors for the individual and simultaneous detection of heavy metal ions.

Conflicts of interest

There are no conflicts to declare.

Acknowledgements

The authors are grateful for the support provided by the National Natural Science Foundation of China under grants (51773184), Shanxi '1331 Project' Key Subject Construction, and Shanxi University State Key Laboratory of Quantum Optics and Photonic Devices Foundation of China (KF201806).

References

1 F. Fu and Q. Wang, *J. Environ. Manage.*, 2011, **92**, 407–418.
2 M. B. Gumpua, S. Sethuraman, U. M. Krishnan and J. B. B. Rayappan, *Sens. Actuators, B*, 2015, **213**, 515–533.
3 S. Chaiyo, E. Mehmeti, K. Zagar and W. Siangproh, *Anal. Chim. Acta*, 2016, **918**, 26–34.
4 B. K. Bansoda, T. Kumarb, R. Thakurc and S. Rana, *Biosens. Bioelectron.*, 2017, **94**, 443–455.
5 G. Aragay and A. Merkoc, *Electrochim. Acta*, 2012, 8449–8461.
6 Y. Y. Sun, W. H. Zhang, H. L. Yu and C. l. Hou, *J. Alloys Compd.*, 2015, **638**, 182–187.
7 S. B. Sang, D. Li, H. Zhang and Y. Y. Sun, *RSC Adv.*, 2017, **7**, 21618–21624.
8 S. F. Zhou, J. J. Wang, L. Gan and X. J. Han, *J. Alloys Compd.*, 2017, **721**, 492–500.
9 Y. F. Sun, L. J. Zhao, T. J. Jiang and S. S. Li, *J. Electroanal. Chem.*, 2016, **760**, 143–150.
10 J. Z. Huang, S. L. Bai, G. Q. Yue and W. X. Cheng, *RSC Adv.*, 2017, **7**, 28556–28563.
11 Q. X. Zhang, H. Wen, D. Peng and Q. Fu, *J. Electroanal. Chem.*, 2015, **739**, 89–96.
12 F. G. Xu, F. Wang, D. G. Yang and Y. Gao, *Mater. Sci. Eng., C*, 2014, **38**, 292–298.
13 C. Yan, Z. S. Li and Z. G. Zou, *Langmuir*, 2009, **25**, 10397–10401.
14 G. P. Dong, Y. H. Zhang, Q. W. Pan and J. R. Qiu, *J. Photochem. Photobiol., C*, 2014, **20**, 33–50.
15 C. C. Shen, C. L. Chen, T. Wen and Z. W. Zhao, *J. Colloid Interface Sci.*, 2015, **456**, 7–14.
16 S. L. Ma, S. H. Zhan, Y. N. Jia and Q. Shi, *Appl. Catal., B*, 2016, **186**, 77–87.
17 C. Zhang, Y. Y. Zhou, L. Tang and G. M. Zeng, *Nanomaterials*, 2016, **6**, 1–11.
18 R. Hu, X. k. Wang, S. Y. Dai and D. D. Shao, *Chem. Eng. J.*, 2015, **260**, 469–477.
19 S. W. Zhang, J. X. Li, M. Y. Zeng and J. Z. Xu, *Nanoscale*, 2014, **6**, 4157–4162.
20 S. Z. Guo, N. Duan, Z. G. Dan and G. Y. Chen, *J. Mol. Liq.*, 2018, **3**, 1–41.
21 S. Z. Hua, L. Ma, J. G. You and F. Y. Li, *Appl. Surf. Sci.*, 2014, **311**, 164–171.
22 L. Pi, R. Jiang, W. C. Zhou and H. Zhu, *Appl. Surf. Sci.*, 2015, **8**, 1–9.
23 X. J. She, H. Xu, Y. G. Xu and J. Yan, *J. Mater. Chem. A*, 2013, **3**, 1–9.
24 D. P. Wang, Y. Tang and W. D. Zhang, *Microchim. Acta*, 2013, **7**, 1007–1013.
25 Q. Zhang, Q. T. Huang, Y. H. Huang and F. M. Li, *Electrochim. Acta*, 2014, **142**, 125–131.
26 X. G. Chai, J. Y. He, L. Chen and K. Chen, *Chemosphere*, 2017, **171**, 192–201.
27 G. Mamba and A. K. Mishra, *Appl. Catal., B*, 2016, **198**, 347–377.
28 Q. Y. Lin, L. Li, S. J. Liang and M. H. Liu, *Appl. Catal., B*, 2015, **163**, 135–142.
29 Z. C. Sun, Z. Q. Yu, Y. Y. Liu and C. Shi, *J. Colloid Interface Sci.*, 2018, **533**, 251–258.
30 M. Anbia and M. Haqshenas, *J. Iran. Chem. Soc.*, 2014, **2**, 424–431.
31 D. Peng, W. Jiang, F. F. Li and L. Zhang, *ACS Sustainable Chem. Eng.*, 2018, **7**, 1–31.
32 H. Y. Lv, Z. Y. Teng, C. Y. Wang and G. X. Wang, *Sens. Actuators, B*, 2016, **9**, 1–7.
33 Y. C. Deng, L. Tang, G. M Zeng and Z. J. Zhu, *Appl. Catal., B*, 2017, **203**, 343–354.
34 Y. Wang, Q. Xia, B. Xia, Z. G. Ge and Q. Yang, *Appl. Catal., B*, 2018, **8**, 1–35.
35 W. Y. Gao, X. F. Wang, P. Li and Q. T. Wu, *RSC Adv.*, 2016, **1**, 1–6.
36 H. Y. Lv, Z. Y. Teng, C. Y. Wang and G. X. Wang, *Sens. Actuators, B*, 2016, **9**, 1–7.
37 Q. J. Fan, Y. N. Huang, C. Zhang and J. J. Liu, *Catal. Today*, 2016, **264**, 250–256.
38 B. Choudhury and P. K. Gir, *RSC Adv.*, 2016, **6**, 24976–24984.
39 S. Ding and A. Ali, *Materials*, 2018, **11**, 1–16.
40 Z. Y. Teng, H. Y. Lv, L. N. Wang and L. Liu, *Electrochim. Acta*, 2016, **212**, 722–733.
41 Y. Wei, Z. G. Liu, X. Y. Yu and L. Wang, *Electrochem. Commun.*, 2011, **13**, 1506–1509.
42 S. Duan and Y. M. Huang, *J. Electroanal. Chem.*, 2017, **807**, 253–260.
43 Q. X. Zhang, D. Peng and X. J. Huang, *Electrochem. Commun.*, 2013, **34**, 270–273.
44 R. X. Xu, X. Y. Yu, C. Gao and Y. J. Jiang, *Anal. Chim. Acta*, 2013, **790**, 31–38.
45 S. B. Sang, H. Zhang, Y. Y. Sun and A. Q. Jian, *Int. J. Electrochem. Sci.*, 2017, **12**, 1306–1317.
46 T. Hezard, K. Fajerwerg, D. Evrard, V. Colliere, P. Behra and P. Gros, *Electrochim. Acta*, 2012, **73**, 15–22.
47 J. l. Zhang, Z. W. Zhu, J. W. Di, Y. M. Long and W. F. Li, *Electrochim. Acta*, 2015, **186**, 192–200.

